*Pure & Appl. Chem.*, Vol.56, No.1, pp.111-128, 1984.
Printed in Great Britain.

0033-4545/84 $3.00+0.00
Pergamon Press Ltd.


# ACTIVATION OF DIHYDROGEN AND METHANE BY PHOTOEXCITED MANGANESE AND IRON ATOMS IN LOW TEMPERATURE MATRICES

Geoffrey A. Ozin*, John G. McCaffrey and Douglas F. McIntosh

Lash Miller Chemistry Laboratories, 80 St. George Street, University of Toronto, Toronto, Ontario, Canada M5S 1A1

Abstract - The photophysical and photochemical consequences of electronically exciting metal atomic reagents in cryogenic matrices containing dihydrogen and methane are delineated and illustrated by reference to some recent observations for Mn and Fe atoms. Photoreversible oxidative-addition/reductive-elimination reactions

$$M + RH \underset{h\nu}{\overset{h\nu}{\rightleftharpoons}} RMH$$

are described for both $H_2$ and $CH_4$ with Mn and Fe atoms. The spectroscopic and kinetic evidence leans heavily towards (i) an activated and concerted photoinsertion of Fe and Mn atoms into $H_2$ and $CH_4$ to form $MH_2$ and $CH_3MH$ having non-linear geometries, and (ii) a non-activated and concerted photoreductive-elimination of Fe and Mn atoms, $H_2$ and $CH_4$ from $MH_2$ and $CH_3MH$. The SCF-X$\alpha$-SW molecular orbitals for non-linear $FeH_2$ are computed in order to determine which excited state(s) could be responsible for the observed photoreductive-elimination reaction. The insertion of an excited metal atom into the C-H bond of $CH_4$, is modelled with the $^2P$ state of Li. A series of geometry optimizations are performed for apex ($C_{3v}$), edge ($C_{2v}$), face ($C_{3v}$) and edge ($C_s$) attack of $^2P$ Li on $CH_4$ in order to locate a possible transition state. The reaction pathway with the lowest energy is via the A' state of an edge $C_s$ attack model. The activation barrier to insertion involves elongation of a C-H bond to form a species in which the H atom is essentially abstracted giving a $CH_3$ radical and LiH, which subsequently relax to form $CH_3$... LiH stabilized by the "single electron bond" between the methyl and lithium hydride moieties.

## INTRODUCTION

The cleavage of C-H and H-H bonds in saturated hydrocarbons and dihydrogen mediated by metal atom sites in mononuclear and polynuclear molecular complexes, supported metal clusters and metal surfaces are fundamental reactions in organometallic chemistry, heterogeneous catalysis and surface chemistry and play key roles in several homogeneous and heterogeneous catalytic industrial processes (Ref.1,2,3).

The delineation of reaction profiles and the determination of thermodynamic, electronic and geometrical factors for C-H and H-H bond reactions at metal atom sites presents both an experimental and theoretical challenge which impinges on a number of questions. These include, symmetry based electronic state correlations between reactants, reactive intermediates, transition states and products; activation barriers and kinetic isotope effects as a probe of the transition state; matching of $\sigma/\sigma^*$ C-H and H-H levels with metal orbitals as function of dsp occupation and the nature of the metal site; geometrical features, electronic structure, bonding properties and proximity effects prior to, during and following the bond activation step.

The microscopically reversible reductive-eliminaiton and desorption reactions at metal atom sites are of equal importance in the understanding of a number of catalytic phenomena involving saturated hydrocarbons and dihydrogen (Ref. 1,2,3).

A definitive characterization of the multitude of factors involved in RH and $H_2$ chemisorption/desorption processes at metal surfaces and oxidative-addition/reductive-elimination reactions on metal complexes has not yet proven feasible. This is partly due to the complexity of these systems and the difficulty of extracting atomic and molecular detail at the active metal site. In this situation one would ideally like to explore insertion and elimination steps in a "ligand-free" $Mn + RH \rightleftharpoons RMnH$ (where R = $CH_3$ or H) model reversible system as a function of the nuclearity n, shape and nature of M. The inherent molecular simplicity of the mononuclear species $CH_3MH$ and $MH_2$ confers to them the desirable qualities required for detailed spectroscopic and structural investigations backed by quantum chemical calculations.

Up to now however, experimental methods for exploring M + RH $\rightleftharpoons$ RMH reversible C-H and H-H bond activation reactions had not previously been reported. A new method for achieving this important goal forms the main thrust of this paper. With these systems it is now feasible to conduct detailed experimental and theoretical investigations on two of the most fundamental steps in homogeneous and heterogeneous catalysis involving alkanes and dihydrogen (Ref. 1,2,3).

## EXCITED STATE METAL ATOM CHEMISTRY; THERMODYNAMIC AND KINETIC CONSIDERATIONS.

A large number of reactions involving ground state metal atomic reagents can be conducted in the range 4.2 - 40K (low activation barrier processes, thermally assisted by metal atom translational energies, matrix/ligand condensation energies and metal source radiation energies, 3-5 kcal $mol^{-1}$). The major products formed in these systems usually arise from low activation energy, simple orbital mixing processes such as:

| | |
|---|---|
| $Pt + CO \rightarrow Pt(CO)_4$ | (Ref. 4) |
| $Ni + N_2 \rightarrow Ni(N_2)_4$ | (Ref. 5) |
| $Rh + O_2 \rightarrow Rh(O_2)_2$ | (Ref. 6) |
| $Cu + C_2H_4 \rightarrow Cu(C_2H_4)_3$ | (Ref. 7) |
| $Ni + C_2H_2 \rightarrow Ni(C_2H_2)_2$ | (Ref. 8) |
| $Cr + Mo \rightarrow CrMo$ | (Ref. 9) |

However, there is a fairly large "unreactive" metal atom/ligand group that simply leads to matrix samples comprising metal atoms isolated in unreacted ligand. Reactions involving ground state metal atom induced bond cleavage processes, such as those found in the oxidative-addition

$$M + RH \rightarrow RMH$$

fall in the above class and do not usually proceed at 4.2 - 40K. It is specifically this class of ligands, namely those that are unreactive towards ground electronic state metal atomic reagents at 4.2 - 40K that this paper addresses.

In what follows we will briefly contemplate some of the more interesting photophysical and photochemical consequences of electronically exciting metal atomic reagents in cryogenic matrices containing dihydrogen and methane, which are well known to be "inert" towards transition metal atoms in their ground electronic state at 4.2 - 40K.

In general terms, the basic physical and chemical mechanisms whereby fluorescence from the lowest M* and M** excited states of metal atoms is quenched by RH (where R = $CH_3$ or H) are illustrated in the energy level scheme of Figure 1. From this picture, one can determine that the reaction of M with RH to give the insertion product RMH is sufficiently endothermic not to proceed at a measurable rate at 4.2 - 40K. (The only reported exception to this rule is $Al(^2P)/CH_4$ which leads to $CH_3AlH$, (Ref. 10)). However, with respect to selected

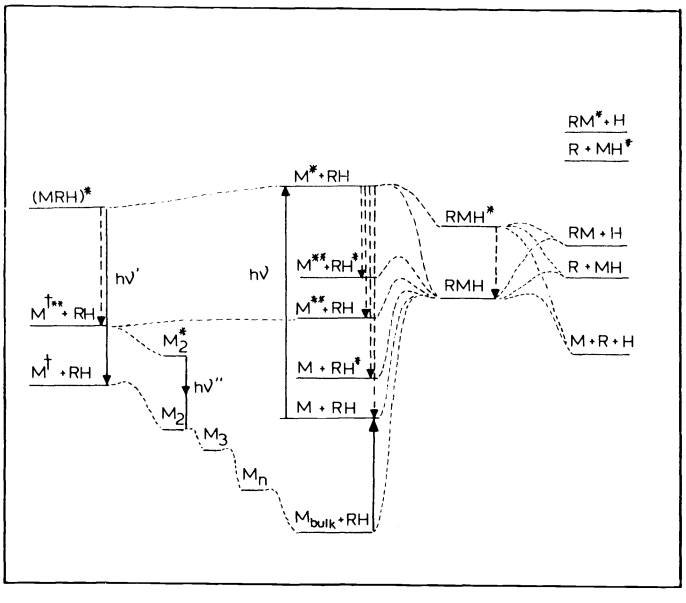


Figure 1 - A schematic view of condensed phase energetics, dynamics and reaction pathways of ground and excited electronic state metal atoms with alkanes and dihydrogen

electronically excited states M* and M**, the situation can be dramatically altered. Thus provided that there exists no insurmountable steric barriers, spin-selection rules or orbital symmetry constraints, the reaction of M* or M** to yield RMH, will likely be exothermic or at least thermoneutral, with either a zero or small activation barrier and hence will proceed at a measureable rate at 4.2 - 40K. Whether RMH is directly formed in its electronic ground state or an excited state (which may be unstable with respect to fragmentation Figure 1) will depend intimately on the precise mechanism of chemical quenching of M* and M** and the atomic state involved.

Aside from formation of the RMH insertion product (Figure 1), another chemical quenching process of M* that can compete with the RMH reaction involves vibrational relaxation of the matrix cage atoms or molecules around M* (Jahn-Teller effect, exciplex formation) followed by radiative and/or non-radiative decay to the ground state M. The destabilization caused by producing a ground state (MRH) "cage-complex" in the relaxed excited state configuration can provide the driving force for photoinduced diffusion of ground state M atoms and subsequent aggregation to $M_2$, $M_3$, $M_4$ etc. metal clusters (Figure 1). Alternatively, M* can relax non-radiatively to a lower energy electronically excited state M** atom. The energy thereby released into the matrix in this process could cause "local softening" of the surrounding cage, resulting in photoinduced diffusion of M**† (e.g. long lived mobile excited state) and reactive encounters with nearby ground state M atoms forming $M_2$, $M_3$, $M_4$ etc. metal clusters (Figure 1). The metal atom photoaggregation phenomenon involving both ground and electronically excited state metal atoms has been documented for Na, Cu, Ag, Cr, Mo and Rh atoms (Ref. 11).

In what follows, selected physical and chemical aspects of the photochemistry of matrix isolated transition metals as well as their reaction products, of the kind depicted in Figure 1, will be briefly illustrated by reference to some recent observations for electronically excited Mn and Fe atoms with $H_2$ and $CH_4$. Part of this work has been reported previously. For background details of the research the original literature references should be consulted.

## ACTIVATION OF DIHYDROGEN BY PHOTOEXCITED Mn AND Fe ATOMS IN LOW TEMPERATURE MATRICES

Let us begin this discussion by reference to Fe atoms and then extend the idea to Mn. The optical spectra of iron atoms entrapped in 10% $H_2$/rare gas matrices can be readily correlated with those of iron atoms in the gas phase (using the AMCOR technique of Gruen (Ref. 12), experimental support for which is now accessible from matrix MCD spectroscopy (Ref.13). The 307 nm ($3d^64s^14p^1$, $^5P_3 \leftarrow 3d^64s^24p^0$, $^5D_4$) Fe atom quenching kinetics were found to be pseudo first order and roughly five times faster in $H_2$/Xe than in $D_2$/Xe matrices at 12K. Optical absorptions associated with photoproducts were observed to grow in at 400, 419 and 441 nm in $H_2$/Xe matrices (Figure 2) which showed small deuterium shifts to 402, 420 and 439 nm, indicating that these new absorptions are associated with an iron-hydrogen containing product (Ref. 14).

The corresponding infrared experiments led to the identification of an iron-hydrogen containing species absorbing at 1636 and 323 $cm^{-1}$ in $H_2$/Xe and 1188 and 232 $cm^{-1}$ in $D_2$/Xe matrices (Figure 3). The analogous experiments in HD/Xe matrices show the respective stretching and deformational modes at 1665, 1198 and 280 $cm^{-1}$ (Figure 3) which is the isotopic pattern expected for a FeHD insertion product rather than that of a molecular dihydrogen complex Fe(HD), thereby specifying the photochemical pathway to an iron dihydride. The weak bands labelled a and a' at 1660 $cm^{-1}$ and 1204 $cm^{-1}$ (Figure 3) which are associated with $FeH_2$ and $FeD_2$ respectively and which absorb at slightly higher frequencies than the asymmetric $\nu FeH_2$ and $\nu FeD_2$ stretching modes are clearly absent in FeHD. They are therefore best ascribed to the symmetrical $\nu FeH_2$ and $\nu FeD_2$ stretching modes, rather than with a secondary trapping site of iron dihydride (cf $MnH_2$ later) and hence evidence for a non-linear geometry. The low intensity shoulders denoted b and b' (Figure 3) do on the other hand behave as a multiple trapping site of $FeH_2$ and $FeD_2$ respectively,and have been assigned accordingly. The ratio of the infrared intensities of the stretching modes of $FeH_2$ (bond dipole model) is given by $I_{B_2}/I_{A_1} = \tan^2\theta/2$, where $\theta$ is the apical angle. This yields a value of around 120° for $FeH_2$ (see later).

The corresponding infrared spectra recorded in $Fe/H_2/D_2/Xe$ mixed isotopic matrices display only those absorptions associated with $FeH_2$ and $FeD_2$ with no evidence for scrambling as seen by the spectroscopic absence of FeHD. In the $H_2/D_2$/Xe matrices, $FeH_2$ is found to form preferentially over $FeD_2$ by a factor of 5.76 (IR absorbance measurements on the stretching modes, Figure 3E). As expected, this parallels the approximately five times faster bleaching rate for 307 nm photoexcited Fe atoms in $H_2$/Xe compared to $D_2$/Xe matrices (vide infra). Note that for a pseudo first order competitive insertion reaction:

$$M^* + H_2 + D_2 \longrightarrow MH_2 + MD_2$$

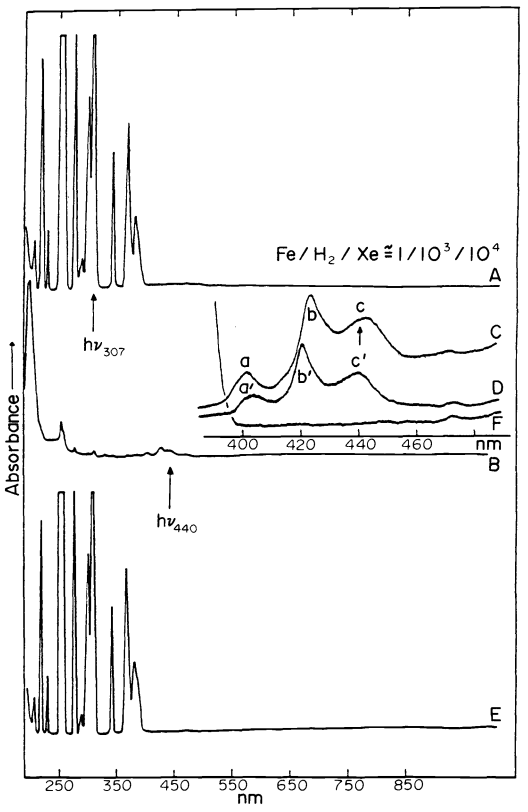


Figure 2 - The optical spectra of a freshly deposited (A) $Fe/H_2/Xe \cong 1/10^3/10^4$ 12K matrix (B) following 45 min. 307 nm atomic Fe photolysis (C) scale expansion of 380-480 nm region of (B),(D) scale expansion of the $Fe/D_2/Xe \cong 1/10^3/10^4$ analogue of (C), (E) the matrix sample shown in (B) following 15 min. 440 nm $FeH_2$ photolysis. The $FeH_2$ and $FeD_2$ product bands are denoted a , b , c and a',b',c' respectively (Ref.14).

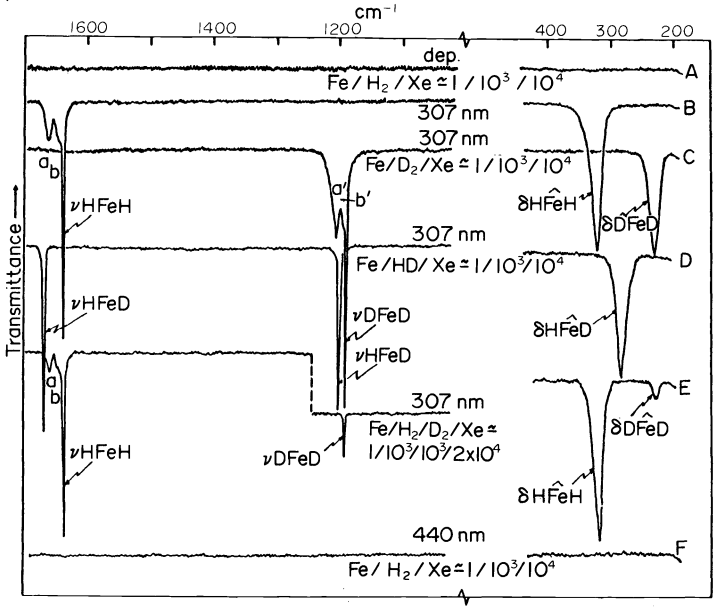


Figure 3 - Infrared spectra of (A) a freshly deposited $Fe/H_2/Xe \cong 1/10^3/10^4$ 12K matrix (B) following 120 min. 307 nm atomic iron photolysis and the same for (C) $Fe/D_2/Xe \cong 1/10^3/10^4$ (D) $Fe/HD/Xe \cong 1/10^3/10^4$ (E) $Fe/H_2/D_2/Xe \cong 1/10^3/10^3/2x10^4$ and (F) the matrix sample shown in (B) following 30 min. 440 nm $FeH_2$ photolysis. The stretching and deformational modes of $FeH_2$, FeHD and $FeD_2$ are indicated. See text for a discussion of the a,a',b,b' bands. (Ref. 14).

the time dependence of the concentration of the $MH_2$ and $MD_2$ photoproducts is given by:

$$[MH_2] = \left(\frac{k_H}{k_H+k_D}\right) [M_o] (1-\exp[-\tfrac{1}{2}(k_H+k_D)t])$$

$$[MD_2] = \left(\frac{k_D}{k_H+k_D}\right) [M_o] (1-\exp[-\tfrac{1}{2}(k_H+k_D)t])$$

which leads in one experiment (rather than two separate M* + $H_2$ and M* + $D_2$ experiments) directly to $k_H/k_D = [MH_2]/[MD_2]$, thus mirroring the ln[Fe] versus photolysis time t behaviour in $H_2/X_2$ and $D_2$/Xe matrices (vide infra). The observation of a substantial kinetic isotope effect for the Fe*/$H_2$ reaction alerts one to the existence of an activation barrier for the insertion step. Taking into account the low temperature at which the reaction is performed (zero point energy and possibly tunnelling corrections) the observed $k_H/k_D$ isotope ratio of around 5-6 for the Fe*/$H_2$ reaction,translates into a $k_H/k_D$ ratio of around 1.11 - 1.13 at ambient temperatures which would indicate a small degree of H-H stretching in an "early" transition state and probably a low activation barrier for insertion. These observations are in line with theoretical studies of $H_2$ oxidative-addition to $Pt(PH_3)_2$ which have indicated about 4-18% stretching of the H-H bond in the transition state (Ref. 15a), experimental data for $H_2$ addition to a metal centre in molecular $ML_n$ complexes which show a $k_H/k_D$ isotope ratio of 1.2 - 1.3 (Ref. 15b) and neutron diffraction data for the H-H bond length in the first example of a molecular hydrogen complex, $W(CO)_3(PPr^i_3)_2(\eta^2-H_2)$, at 0·75 Å compared to gaseous $H_2$ at 0·74 Å (Ref. 15c).

In the Fe*/$H_2$/Xe reaction there was no sign of FeH or $FeH_x$ ($x \geq 3$) in the infrared experiments, nor H-atoms in the analogous esr experiments. In general similar results were found for $^6P(3d^54s^14p^1) \leftarrow {}^6S(3d^54s^2)$,285 nm photoexcited Mn atoms in $H_2$/Xe matrices (Ref. 16). The spectroscopic results are summarized in Figures 4,5 and Table I. The only differences worth mentioning at this point, is the definite existence of $MnH_2$ in two distinct trapping sites (denoted A and B in Figure 5) and the preferential formation of $MnH_2$ over that of $MnD_2$ in $H_2/D_2$/Xe = 1/1/20 matrices (Figure 5E, absorbance measurements) by a factor of around three. The significance of these $k_H/k_D$ differences between the Fe*/$H_2$/Xe and

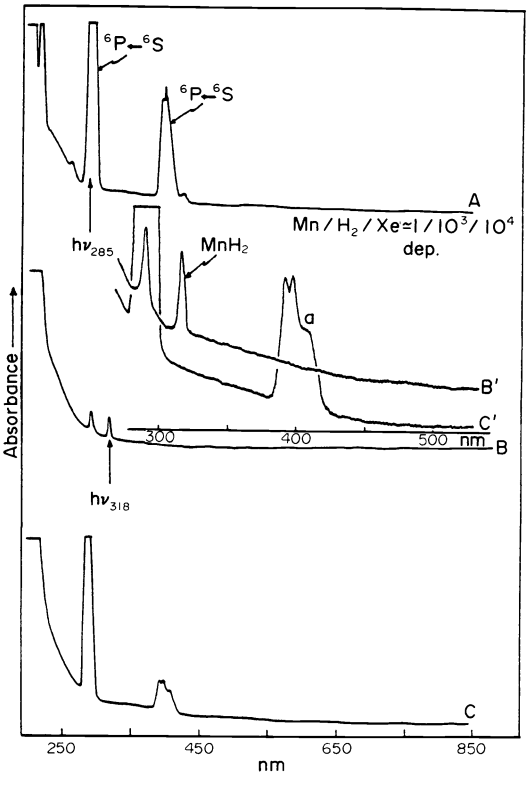


Figure 4 - The optical spectra of (A) freshly deposited $Mn/H_2/Xe \cong 1/10^3/10^4$ matrices at 12K (B) following 60 min. 285 nm photolysis of (A), (C) following 15 min. 318 nm photolysis of (B), (B') and (C') are scale expansions of (B) and (C) respectively (Ref. 16).

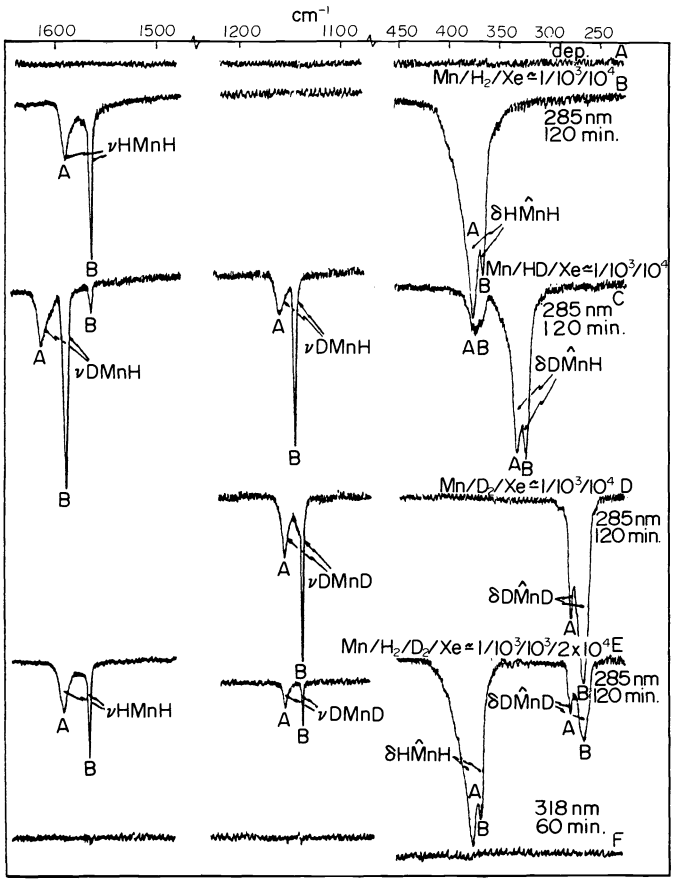


Figure 5 - The infrared spectrum of (A) freshly deposited $Mn/H_2/Xe \cong 1/10^3/10^4$ matrices at 12K (B) following 120 minutes 285 nm photolysis of (A), (C) the same as (B) but for $Mn/HD/Xe \cong 1/10^3/10^4$, (D) the same as (B) but for $Mn/D2/Xe \cong 1/10^3/10^4$, (E) the same as (B) but for $Mn/H_2/D_2/X_2 \cong 1/10^3/10^3/2x10^4$ (F) following 20 min.318 nm photolysis of (B),(Ref. 16).

TABLE 1. Infrared spectra[a] for $MH_2$, (where M = Mn,Fe) isolated in solid xenon ($cm^{-1}$)

| $MnH_2$ | $FeH_2$ | Tentative Mode Assignment |
|---|---|---|
| | 1660 | $\nu$sym $MH_2$ |
| 1591/1565[b] | 1636 | $\nu$asym $MH_2$ |
| 375/366[b] | 323 | $\delta$ $MH_2$ |

a Ref. 14,16.
b Ascribed to $MnH_2$ trapped in two slightly different matrix sites.

$Mn^*/H_2/Xe$ photoinsertion reactions is still under investigation.

The accumulated spectroscopic and kinetic evidence therefore strongly suggests an activated and concerted insertion of 307 nm and 285 nm photoexcited Fe and Mn atoms into the hydrogen bond of $H_2$ to form $FeH_2$ and $MnH_2$ respectively, probably having non-linear geometries (see later, on the subject of reductive elimination), with no detectable participation of a molecular dihydrogen complex, $M(H_2)$, nor indication of competing H-atom abstraction, secondary photolysis channels, formation of higher metal hydrides, $MH_x$, ($x \geq 3$), nor photoaggregation processes.

PHOTOREDUCTIVE ELIMINATION: THE $MH_2 \xrightarrow[12K]{h\nu} M + H_2$ MATRIX PHASE REACTION FOR M = Mn OR Fe

In this discussion we will consider experimental and theoretical aspects of the photoreactivity of $FeH_2$ and $MnH_2$ insertion products, generated cleanly and efficiently by 307 nm and 285 nm excitation of Fe and Mn atoms co-isolated with $H_2$ in low temperature matrices (Ref. 14,16). We will begin by reference to Fe atoms and then extend the idea to Mn atoms.

The uv-visible and infrared spectra both depict the monotonic bleaching of the $FeH_2$ absorptions with 440 nm irradiation time (Figure 2,3). Of particular note was the concurrent and rapid generation of atomic iron, clearly seen by the steady growth of the atomic resonance lines in the optical spectrum (Figure 2). During the photoannihilation of $FeH_2$, neither infrared nor ESR bands characteristic of FeH or H atoms or $FeH_x$, ($x \geq 3$) were ever observed. Furthermore, the 440 nm photobleaching of $FeH_2$ and $FeD_2$ with concomitant production of Fe atoms was essentially quantitative (Figure 2A, 2E), followed first order kinetics and displayed no measureable kinetic isotope effect.

Similar experiments performed on the 315 nm absorption of $MnH_2$ (Figure 4) also causes rapid bleaching of the uv-visible and infrared bands of $MnH_2$ with concurrent regeneration of the Mn atomic resonance lines (Figure 4C). However, in this case only about 50% of the original Mn atoms can be recovered in this photoreductive-elimination procedure. As there is no evidence for MnH, H or $MnH_x$, ($x \geq 3$) in this reverse photolysis reaction, one can only speculate that either some of the original Mn atoms were lost in a catastrophic photonucleation process to higher manganese clusters during the initial photoinsertion step (no $Mn_2$ or $Mn_3$ observed, see later),or less likely that some of the Mn atoms were lost in the photoreductive-elimination step also to higher manganese clusters (no $Mn_2$ or $Mn_3$ observed).

Collectively, the spectroscopic and kinetic evidence argues in favour of a non-activated and concerted reductive-elimination of Fe and Mn atoms from 440 nm and 318 nm photoexcited $FeH_2$ and $MnH_2$, where MH, H, $M(H_2)$ or $MH_x$,($x \geq 3$) reaction intermediates if involved must play a minor role in the reaction as they remained below the detection limits of the analytical methods employed in this study.

It therefore seems likely that 440 nm and 318 nm photoexcitation of $FeH_2$ and $MnH_2$ populates low lying electronic states having antibonding character between the metal-hydrogen bonds and bonding character with respect to the hydrogen bond. In a non-linear configuration this state is probably akin to a three centre


transition state complex, which would be responsible for the low activation energy and concerted reductive-elimination of M and $H_2$ from $FeH_2$ and $MnH_2$. This probably occurs in much the same way as that postulated to occur in the photoinduced-reductive-elimination of $H_2$ from $(\eta^5\text{-}C_5H_5)_2MoH_2$, $IrClH_2(PPh_3)_3$ and $IrH_3(PPh_3)_3$ complexes (Ref. 17).

## SCF-Xα-SW MOLECULAR ORBITAL CALCULATIONS FOR NON-LINEAR $FeH_2$; RELEVANCE TO THE PHOTOREDUCTIVE-ELIMINATION REACTION

In order to gain a deeper understanding of the "ligand-free" $MH_2 \xrightarrow{h\nu} M + H_2$ photoreductive-elimination reactions we have examined the electronic structure of some transition metal dihydrides (Ref. 18). The SCF-Xα-SW MO energy level scheme for $FeH_2$ with an apical angle of 120° (IR intensity estimate) is shown for illustrative purposes in Figure 6. Beginning at lowest energies, one finds the two expected iron-hydrogen σ-bonding orbitals ($1a_1$,$1b_1$) followed at higher energies by a group of almost degenerate,practically pure iron 3d-orbitals ($2a_1$, $3a_1$, $1a_2$). Next in order is a $2b_1$ level which can be considered to be the σ*-antibonding counterpart of the $1b_1$ iron-hydrogen σ-bonding orbital. It has a substantial iron and hydrogen contribution with a node between the iron and hydrogen atoms. At still higher energies one finds the $4a_1$ level which is seen to be the σ*-antibonding counterpart of the $1a_1$ iron-hydrogen σ-bonding orbital, again with nodes between the iron and hydrogen atoms. highest lying $2b_2$ level is essentially pure Fe 4p in character.

It is significant that the optical spectra of $FeH_2$ show at least three low energy absorptions around 400, 419 and 441 nm and that excitation into each of these leads to the clean and facile production of Fe atoms and $H_2$ (Ref. 14). Optical transitions that are computed to fall within this energy range are illustrated in Figure 6. One finds at best four possible candidates calculated to occur at 396, 405, 414 and 509 nm. The latter two excitations involve promotion of $FeH_2$ σ-bonding electrons into essentially localized Fe 3d orbitals and are not expected to be too effective in promoting reductive elimination of Fe atoms and $H_2$. The 396 nm excitation involves promotion of Fe 3d localized electrons into a σ*-antibonding $FeH_2$ orbital and might be responsible for an elimination pathway. On the other hand the 405 nm excitation takes a σ-bonding $FeH_2$ electron and places it in a σ*-antibonding orbital and could be quite effective in promoting the observed photoreductive-elimination reaction. One or more of these excited states might turn out to closely resemble the three-centre


transition state complex, proposed earlier to be responsible for the low activation energy and concerted reductive-elimination of Fe and $H_2$ from $FeH_2$. Further work is underway to

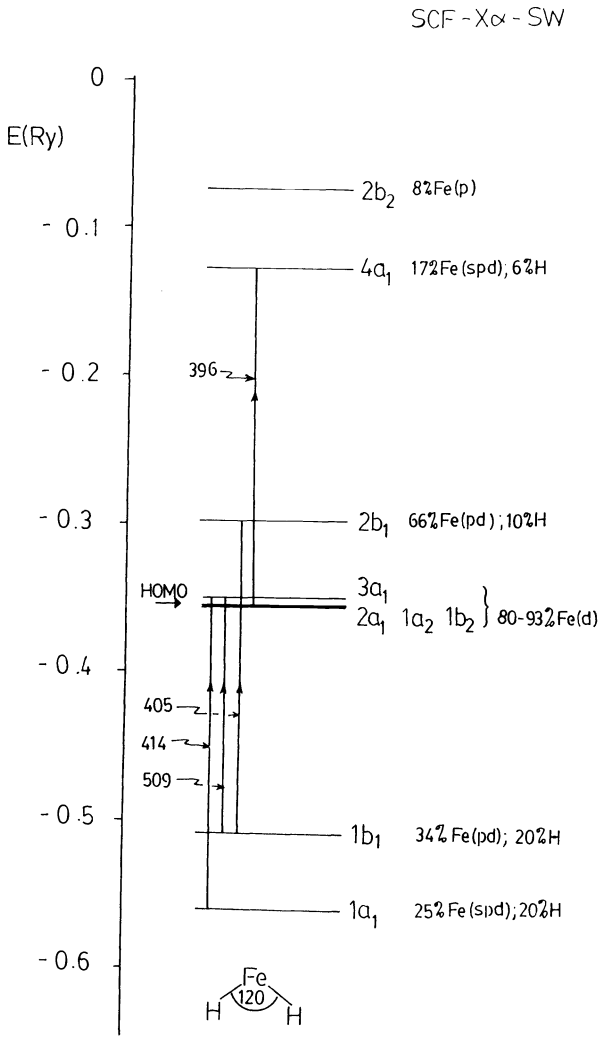


Figure 6 - Ground state spin restricted SCF-Xα-SW molecular orbital scheme for non-linear $C_{2v}$ $FeH_2$ ($\alpha_{Fe}$=0.71151; $\alpha_H$=0.77725; $r_{FeH}$ = 1.77Å; HFeH = 120°). The computed partial wave contributions to the various molecular orbitals are indicated in the energy level diagram as well as the proposed excitations in the 400 - 500 nm region thought to be responsible for the observed optical transitions in this range and the photoreductive-elimination pathway (Ref. 18).

explore this interesting result.

ACTIVATION OF METHANE BY PHOTOEXCITED Mn AND Fe ATOMS IN LOW TEMPERATURE MATRICES

Narrow band irradiation into the intense 285 nm, $^6P(3d^54s^14p^1) \leftarrow {}^6S(3d^54s^2)$ atomic resonance line of Mn atoms in $CH_4$ under high dispersion ($1/10^4$) conditions at 12K (Ref. 19) causes rapid bleaching of all Mn atom lines with concomitant growth of weak absorption around 300 - 330 nm (Figure 7). Recall that similar excitation of $Mn/H_2/Xe$ matrices (Ref. 16) produced a new species absorbing around 315 nm (Figure 4).

The corresponding infrared experiments (Figure 8) clearly demonstrated the production of the $CH_3MnH$ insertion product absorbing strongly at 2924, 2894, 2876, 1582, 1143, 1140, 550, 546, 500, 325, 316 $cm^{-1}$, which is remarkably similar to the infrared spectrum of $CH_3FeH$ produced by photoexciting Fe at the intense 300 nm ($3d^64s^14p^1$, $^5P_3 \leftarrow 3d^64s^2$, $^5D_4$) atomic resonance line in $CH_4$ (Ref. 20) also under high dispersion ($1/10^4$) conditions at 12K (Figure 9 and Table 2). For both $CH_3MnH$ and $CH_3FeH$, the presence of a single intense $\nu_{MH}$ and three $\nu_{CH}$ modes in the metal-hydrogen and methyl stretching regions respectively together argue in favour of a $CH_3MH$ rather than a $CH_2MH_2$, $(CH_3)_2M$ or $CH_3M$ formulation for the $M/CH_4$ photoproducts for Mn and Fe.

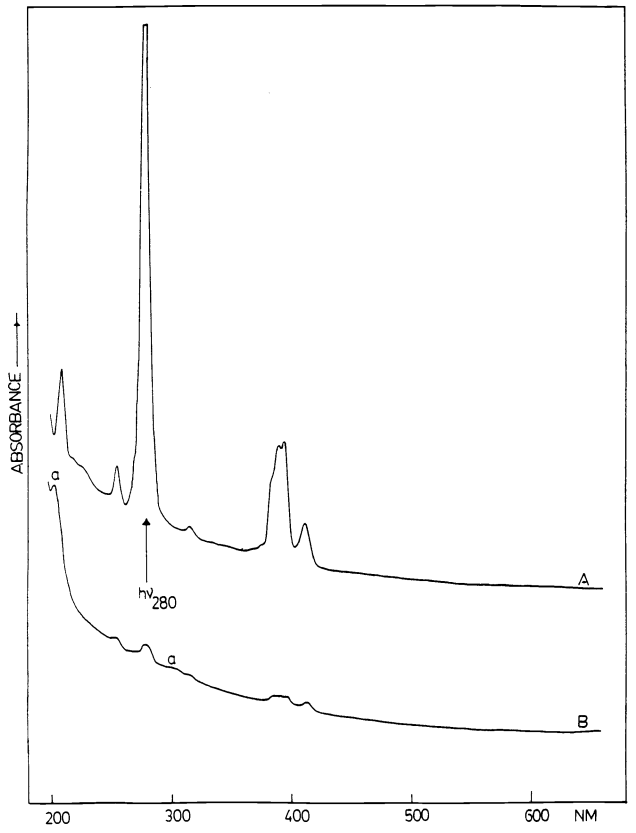


Figure 7 - Optical spectra of (A) freshly deposited Mn atoms in $CH_4$ at 12K ($1/10^4$) and (B) following 25 min. photolysis at 285 nm (Ref. 19).

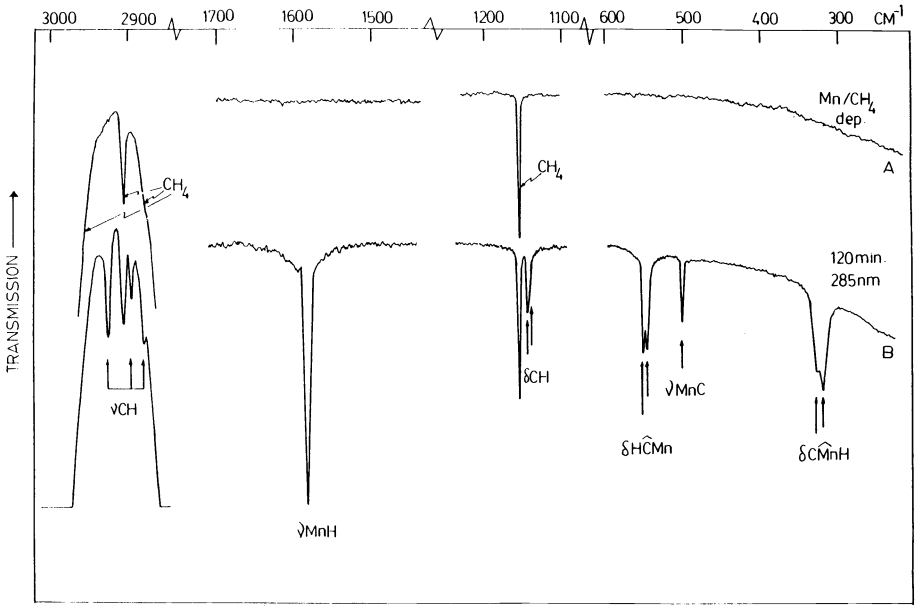


Figure 8 - Inrared spectrum of $Mn/CH_4 \cong 1/10^4$ (A) following deposition at 10-12K showing only $CH_4$ bands (B) following 120 min. photolysis at 285 nm showing $CH_3MnH$ product bands (Ref. 19).

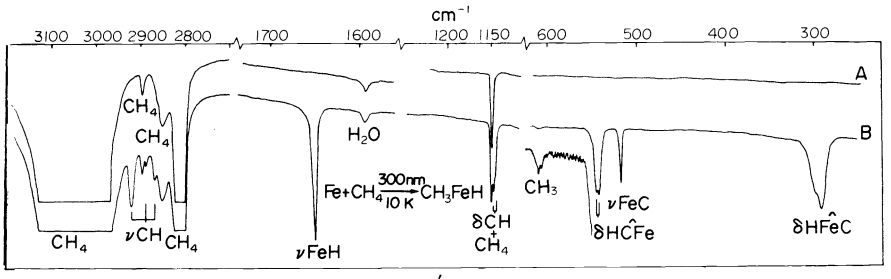


Figure 9 - Infrared spectrum of $Fe/CH_4 \cong 1/10^4$ (A) following deposition at 10-12K showing only $CH_4$ bands (B) following 300 min. photolysis at 300 nm showing $CH_3FeH$ product bands (Ref. 20).

TABLE 2. Infrared spectra[a] for $CH_3MH$, (where M = Mn, Fe) isolated in solid methane ($cm^{-1}$)

| $CH_3MnH$ | $CH_3FeH$ | Tentative Mode Assignment |
|---|---|---|
| 2924 | 2921 | $\nu$ $CH_3$ |
| 2894 | 2888 | $\nu$ $CH_3$ |
| 2876 | 2869 | $\nu$ $CH_3$ |
| 1582 | 1650 | $\nu$ MH |
| 1143 | 1148 | $\delta$ $CH_3$ |
| 1140 | 1145 | $\delta$ $CH_3$ |
| 550 | 547 | $\rho$ $H\hat{C}M$ |
| 546 | 544 | $\rho$ $H\hat{C}M$ |
| 500 | 519 | $\nu$ MC |
| 325 | 300 | $\delta$ $H\hat{M}C$ |
| 316 | 293 | $\delta$ $H\hat{M}C$ |

a. Ref. 19,20.

The thermal reactivity of Mn and Fe atoms with respect to $CH_4$ was also examined in the accessible cryogenic range 10-50K. Up to the temperature that the methane actually sublimed away from the sample window (around 50K) no new infrared or optical bands ascribable to a Mn or Fe atom (or cluster) - $CH_4$ thermal reaction product were ever observed.

## EXCITED STATE REACTIVITY AND SELECTIVITY PATTERNS

Let us briefly consider, in the case of $Mn/CH_4$, the idea of excited state selectivity. From an examination of Figure 7, Mn atoms can be seen to absorb strongly around 285 nm and 395 nm in $CH_4$ matrices. These atomic resonance lines most likely correspond to three different excitations which occur around 279 nm and 403 nm in the gas phase (Ref. 12):

$$^6P_{7/2,\ 5/2,\ 3/2} \leftarrow {}^6S_{5/2}$$

These transitions involve promotion of a Mn 4s electron in the $3d^54s^2$ ground state to a spacially diffuse 4p orbital in the $3d^54s^14p^1$ excited state. The singly occupied 4s and 4p metal atomic orbitals are available for bonding with the $\sigma$-bonding and $\sigma^*$-antibonding molecular orbitals of $CH_4$. Since the $\sigma$-level of $CH_4$ is completely occupied, it is expected that the $M^*(3d/4s) + CH_4(\sigma)$ interaction would lead to a transfer of electron density from the $1t_2$ molecular orbital of $CH_4$ to the 3d/4s atomic orbitals of the excited metal atom.On the other hand, the $\sigma^*$-level of $CH_4$ is unoccupied and, thus, could result in a transfer of charge density from the singly occupied 4p atomic orbital of the excited metal atom to the $2a_1$ molecular orbital of $CH_4$. These combined interactions work in a "synergistic" sense and, overall, lead to a weakening of the C-H bonds. Clearly the symmetry and energy matching of metal atom valence orbitals in excited states with the ground state $\sigma(1t_2)$ and $\sigma^*(2a_1)$ orbitals of $CH_4$ are important factors in attempting to rationalize the reactivity patterns of excited metal atoms with $CH_4$. In the case of the first transition series, it has been observed that photoexcited Ti, V, Cr and Ni atoms do not react with $CH_4$ at low temperatures whereas Mn, Fe, Co, Cu and Zn atoms lead to $HMCH_3$ insertion products (Ref. 19,20, 21, 22). Similar reactivity patterns are presently being observed for reactions with $H_2$. This series can be qualitatively understood in terms of the relative energies of the 3d, 4s and 4p atomic orbitals of the excited metal atoms with respect to those of the $1t_2$ and $2a_1$ molecular orbitals of ground state $CH_4$. Figure 10 illustrates the variation of these eigenvalues across the first transition series, as determined by SCF-X$\alpha$ computations. Except for Cr, Ni and Cu, the energy levels were determined for $3d^n4s^14p^1$ excited state configurations. For these three metals, however, a $3d^n4s^04p^1$ excited state configuration was considered.

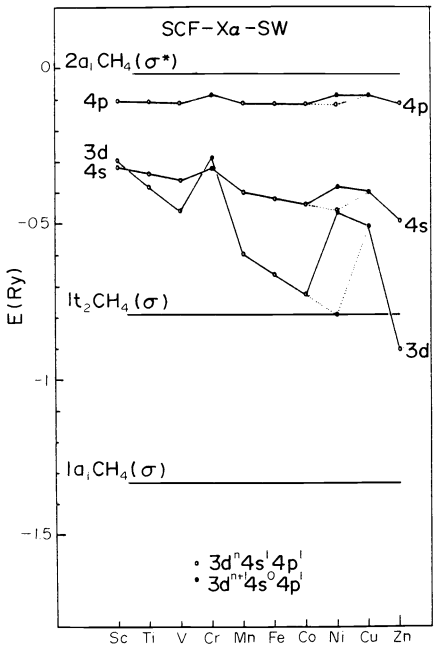


Figure 10 - SCF-Xα-SW Spin Restricted Orbital Energies of $CH_4$ in its Ground Electronic State and the First Transition Series Metal Atoms in Their Low Lying Excited States, $3d^n4s^04p^1$/ $3d^n4s^14p^1$ (Ref. 18).

From the graph, it is clear that the nearly constant values of the 4p energy level for all the excited metal atoms, as well as its proximity to the $2a_1$ energy value of $CH_4$, argues in favour of a relatively similar M*(4p) → $CH_4(\sigma^*)$ interaction for all the first transition metal-atoms. However, there is a dramatic difference among the metal atoms when one considers the M*(3d/4s) - $CH_4(1t_2)$ energy separation. As one passes from Sc to Zn, the 3d and 4s orbitals generally stabilize thereby bringing them closer in energy to the $1t_2$ level of $CH_4$, enhancing their interaction and, presumably, promoting greater charge density donation from $CH_4$ to M*.

Both Cr and Cu have $3d^n4s^14p^0$ ground states in the gas and matrix phases. However, although Ni has a $3d^84s^24p^0$ ground state configuration in the gas phase, recent studies (Ref. 28) on its ground state configuration in various matrix phases have shown that this changes to a $3d^94s^14p^0$ configuration. We have found this to be the case for $CH_4$ as well. This has important consequences when one compares the $3d^84s^14p^1$ excited state of Ni (shown in dotted lines in Figure 10) with the $3d^94s^04p^1$ excited state configuration (solid lines in Figure 10). In the former case, one would expect that the even closer proximity of the 3d and 4s levels of Ni* to the $1t_2$ level of $CH_4$ would result in reaction products, as with those for Mn, Fe, Co, Cu and Zn. In the other case, however, the dramatic destabilization of the 3d and 4s levels of the $3d^94s^04p^1$ excited state of Ni, compared with the alternate excited state eigenvalues or with those of Mn*, Fe* and Co*, could result in anomalous behaviour of Ni and might explain the lack of any observed reaction products when Ni is photoexcited in $CH_4$ matrices.

The above discussion should only be regarded as a preliminary attempt to rationalize the reactivity patterns of electronically excited first transition series atoms with $CH_4$ (similar ideas seem to apply to the results so far obtained for $H_2$ (Ref. 21). Clearly much more work needs to be accomplished in this interesting area before one can begin to appreciate the reactivity characteristics of selected metal atom excited states with $H_2$ and $CH_4$ at low temperatures.

Returning to the question of excited state selectivity. In the case of $Mn/CH_4$ one finds that both 395 nm and 280 nm narrow band excitation of the Mn atoms causes rapid bleaching of the Mn resonance lines with concurrent production of $CH_3MnH$. However, the quenching kinetics are found to have quite different behaviour as seen in Figure 11. For 395 nm photolysis, the Mn atoms follow well behaved pseudo first order decay kinetics whereas 280 nm photolysis results in a much faster bleaching rate, but with neither a first nor second order kinetic dependence (Figure 11). The optical spectra in both cases show no evidence for $Mn_2$ or $Mn_3$ formation and the corresponding infrared spectra depict only the production of $CH_3MnH$ (Ref. 19). Although more experiments need to be done with this system, the preliminary indication is that preparation of the lower energy $^6P$, $3d^64s^14p^1$ state of Mn in $CH_4$ leads cleanly to $CH_3MnH$ in a straight forward first order insertion process:

$$Mn(^6P)^{395} + CH_4 \longrightarrow CH_3MnH$$

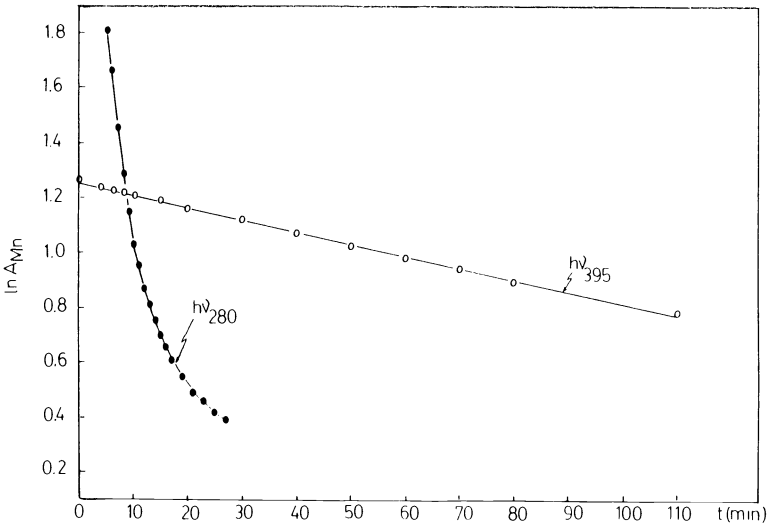


Figure 11 - Kinetic plots between the natural logarithm of the absorbance due to isolated Mn atoms in $CH_4$ at 12K and the cummulative 280 nm and 395 photolysis time (Ref. 21).

as described earlier in Figure 1. On the other hand the higher energy $^6P$, $3d^64s^14p^1$ state of Mn in $CH_4$ appears to be involved in a competing insertion - photoaggregation process:

$$\begin{array}{ccccc} Mn(^6P)^{280} & + CH_4 & \longrightarrow & Mn_x, (x \geq 3) \\ \downarrow & & \searrow^{(A)} & \\ Mn(^6P)^{395} & + CH_4 & \xrightarrow{(B)} & CH_3MnH \end{array}$$

The critical question associated with this 280 nm excitation process, is whether the $CH_3MnH$ product originates directly from the initially prepared 280 nm $^6P$ state (pathway A) or instead arises from the 395 nm $^6P$ state by way of a $^6P285 \rightarrow {}^6P395$ relaxation route (pathway B), or both.

In the context of excited state selectivity, the $Co/H_2/Xe$ has proven to be particularly relevant in that excitation into any of the Russell-Saunders components of the $3d^74s^14p^1 \leftarrow 3d^74s^24p^0$ atomic resonance lines around 247 nm and 257 nm causes photoaggregation to $Co_2$ and $Co_3$ clusters(seen in the uv-visible by the growth of bands around 390, 445 and 530 nm, Ref. 26) but no sign of photoinsertion to $CoH_2$ (infrared spectroscopy). However, photolysis around 342 nm in the region of the lower energy $3d^74s^14p^1 \leftarrow 3d^74s^24p^0$ atomic resonance lines leads to $CoH_2$ absorbing in the infrared at $\nu_{asy}$, 1662 $cm^{-1}$. This implies that for Co in $H_2/Xe$ matrices, relaxation processes from the upper to the lower energy $3d^74s^14p^1$ excited states do not occur,the upper state promoting Co atom clustering while the lower state prefers photoinsertion to $CoH_2$. At this stage of the research it is not immediately clear why two excited states with identical configurations should behave so distinctly. Further studies are underway to more closely examine the important question of excited state selectivity.

## BOND STRENGTH AND GEOMETRY INFORMATION

The importance of metal-hydrogen orbital overlap considerations when considering the early transition metals compared to the later ones can be appreciated from the metal-hydrogen stretching frequency trends for $CH_3MH$ and $MH_2$ species shown in Figure 12. It is well documented that the valence d, s and p-orbitals undergo a significant contraction in the spacial extent of their radial wave functions and that there is a general stabilization of 3d with respect to 4s orbitals with increasing effective nuclear charge (Ref. 27). This would have the effect of increasing M-H bond energies on traversing from the left to the right of a transition series. The metal-hydrogen IR stretching frequency data for $CH_3MH$ and $MH_2$ (where M = Mn, Fe, Co) appear to be reflecting this trend (Figure 12).

Some information pertaining to the geometry of the ground electronic state of $CH_3MnH$ and $CH_3FeH$ can be derived from their infrared spectra. The vibrational spectra of these species are composed of two types of mode, those arising from symmetrical stretching

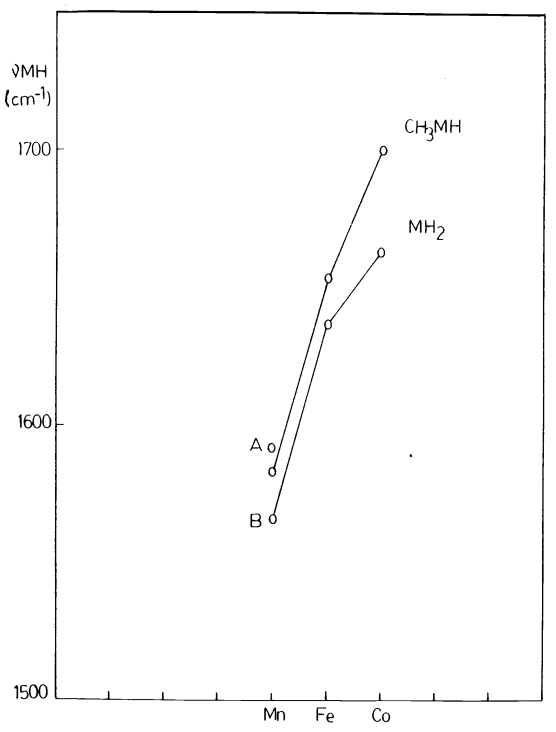


Figure 12 - Graphical representation of the metal-hydrogen IR active stretching frequencies for $CH_3MH$ and $MH_2$ (where M = Mn, Fe, Co). A and B represent either different matrix trapping sites or slightly different geometries of $MnH_2$ (Ref. 14, 16, 19, 20, 21).

and bending motions of CH, MH and MC bonds and those derived from motions that would be doubly degenerate (E) for a linear $C_{3v}$ molecule, while non-degenerate (A' + A") for a non-linear $C_s$ molecule. On the basis that the former modes appear in the IR spectra as sharp singlets, whereas the latter modes are all split into doublets (Figures 8, 9; Table 2), it can be tentatively concluded at this stage that a non-linear geometry prevails for both $CH_3MnH$ and $CH_3FeH$ in solid $CH_4$. ($FeH_2$ is also thought to be non-linear, vide infra). Also the observation of a single "normal" $\nu_{MH}$ stretching mode without any sign of a "softened" $\nu CH$ mode (expected to occur in the 2690-2420 $cm^{-1}$ region (Ref. 23)) argues in favour of the formal insertion product I rather than the plausible alternative activated species II:

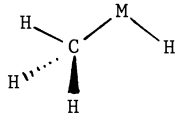


I

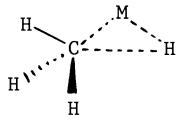


II

PHOTOREDUCTIVE ELIMINATION: THE $CH_3MH \xrightarrow[12K]{h\nu} M + CH_4$ MATRIX PHASE REACTION FOR M = Mn OR Fe.

Let us now focus attention on the 420 nm and 310 nm photoreactivity of the $CH_3FeH$ and $CH_3MnH$ insertion products, generated from 300 nm and 285 nm excitation of Fe and Mn atoms in $CH_4$ under rigorously monatomic conditions (Ref. 19,20). The outcome was probed by both uv-visible and infrared spectroscopy. Concentrating on $CH_3FeH$, one finds that both experiments show monotonic bleaching of the $CH_3FeH$ absorptions with irradiation time at 420 nm (Figure 13H-13K). Especially noteworthy is the concurrent and rapid generation of atomic iron, clearly seen by the steady growth of the atomic resonance lines in the optical spectrum, (Figure 13D-13G). Infrared bands characteristic of new photoproducts were not observed at anytime during the photoannihilation of $CH_3FeH$. The 420 nm photoproduction of Fe atoms from $CH_3FeH$ is found to be highly efficient and essentially quantitative (in our best experiments to date) in terms of the ability to fully recover the Fe atoms consumed in the original 300nm photogeneration of $CH_3FeH$. Similar results were found for $CH_3MnH$ excited

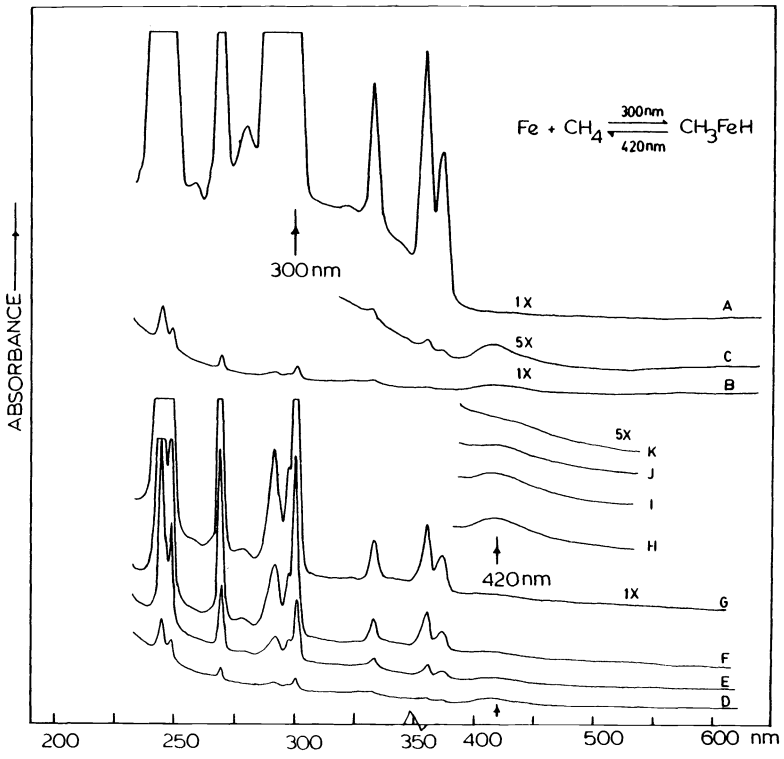


Figure 13 - Uv-visible spectra (A) of Fe atoms isolated in solid $CH_4$ ($1/10^4$) at 10-12K (B) following 30 min. photolysis at 300 nm (C) 5x ordinate expansion of (B) in the 300-600 nm region (D)-(G) samples similar to (B) at 0, 2, 7 and 12 min. photolysis at 420 nm, (H)-(K) 5x ordinate expansion of (D)-(G) in the 370-540 nm region (Ref. 20).

around 310 nm (Figure 7), although the Mn atom recovery was not as efficient as that found for Fe, presumably because of 280 nm Mn atom competing photoagglomeration pathways in solid $CH_4$, vida infra.

In a similar vein to that discussed earlier for the photoreductive-elimination of $M+H_2$ from $MH_2$, one can surmise that 420 nm and 310 nm photoexcitation of non-linear $CH_3FeH$ and $CH_3MnH$, populates a low lying electronic state having antibonding character with respect to the metal-hydrogen and metal-carbon bonds and bonding character between the respective carbon-hydrogen bond. In a non-linear configuration this state probably resembles a three centre transition state complex (Figure 14) and could lead to a facile and concerted reductive-elimination of M and $CH_4$.

The photoinduced reductive-elimination of M and $CH_4$ from $CH_3MH$ and M and $H_2$ from $MH_2$ can be viewed as the microscopic reverse of the photoinsertion of M atoms into the C-H and H-H bonds of $CH_4$ and $H_2$ to produce $CH_3MH$ and $MH_2$ respectively (Figure 14).

These systems therefore provide the first documented cases of "ligand-free" models with which to experimentally probe the individual steps in two of the most fundamental reactions in homogeneous and heterogeneous catalysis and surface chemistry involving methane and di-hydrogen. They also permit one to theoretically evaluate which physically interpretable features of the local electronic structure of the metal, determine chemical reactivity in M/alkane and M/dihydrogen systems.

## AB INITIO SCF CALCULATION OF METAL ATOM INSERTION INTO A C-H BOND OF METHANE

In a first attempt to theoretically probe the insertion of an excited metal atom into a C-H bond of $CH_4$, the $^2P$ state of Li was examined (open shell, restricted Hartree Fock formalism) as a model for the related $^2P$ state of Cu, the latter having been found to produce $CH_3CuH$ in solid $CH_4$ at 12K (Ref. 23,24). In brief the ground state of $CH_3LiH$ was found to be linear $C_{3v}$ with a $^2A_1$ electronic configuration.

In this state $CH_3LiH$ is best described as two weakly interacting parts, a methyl and lithium hydride $CH_3....LiH$, where the long C....Li bond (2.48Å) can be taken as a "single

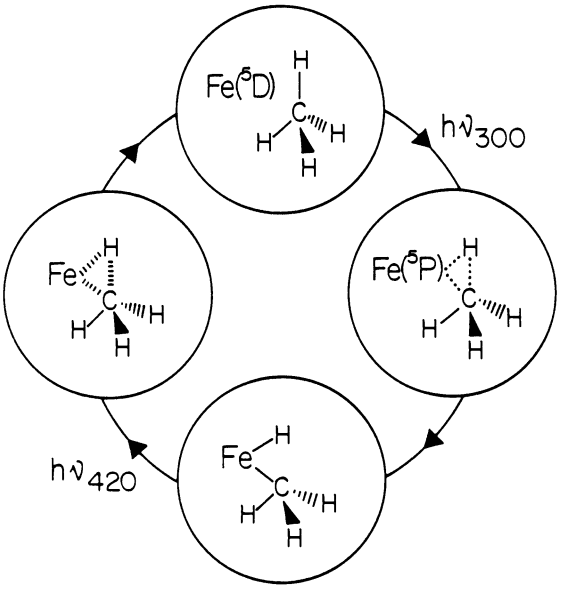


Figure 14 - Illustration of the 300 nm photooxidative- addition of Fe atoms to $CH_4$, and 420 nm photoreductive-elimination of Fe atoms and $CH_4$ from $CH_3FeH$ (Ref. 20).

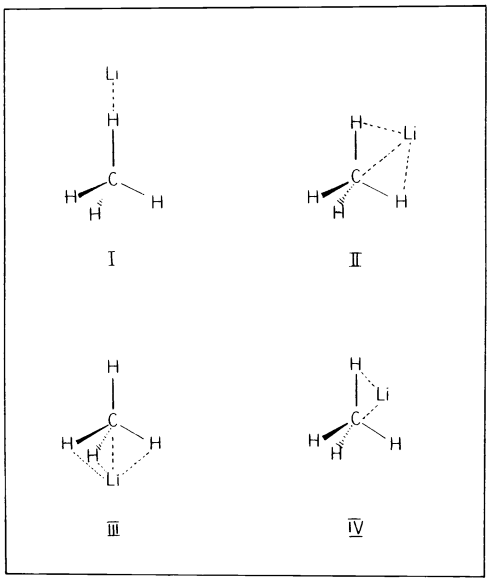


Figure 15 - Possible geometrical arrangements of attack of a Li atom with respect to a $CH_4$ molecule; (I) end-on, $C_{3v}$ (II) side-on, $C_{2v}$, (III) face-on, $C_{3v}$, (IV) side-on, $C_s$ (Ref.24).

electron bond" (cf $CH_3$...LiCl, (Ref. 25) and $CH_3$...CuH, (Ref. 22). The higher excited $^2E$ states show greater interaction of these two parts r(LiC) = 2.18Å with less C-H bonding.

An investigation was made into possible mechanisms for the insertion of a $^2P$ lithium atom into the C-H bond of $CH_4$ (Ref. 24). The intermediates investigated were (I) end-on $C_{3v}$ attack, (II) side-on $C_{2v}$ attack, (III) face-on $C_{3v}$ attack and (IV) side-on $C_s$ attack as depicted in Figure 15. Geometry optimization at the 3-21G and STO-3G basis set levels on all the intermediates (I) to (IV) showed the structures to be unstable with the critical Li-C bond length getting longer in (II), (III) and (IV) and Li....H in (I) giving essentially $CH_4$ and Li as two isolated species.

From the results of a series of single point calculations carried out on the ground and excited states of the various possible insertion geometries, it was found that the reaction pathway with the lowest energy was via the A' state of the side-on $C_s$ attack model (IV). A series of geometry optimizations were performed using the minimization of sum of squares (VA 05 AD) technique in order to locate a possible transition state which corresponds to a first order saddle point on the potential energy hypersurface. The results of the calculations for the A' state show a tendency towards a species with a long C-Li bond and a long

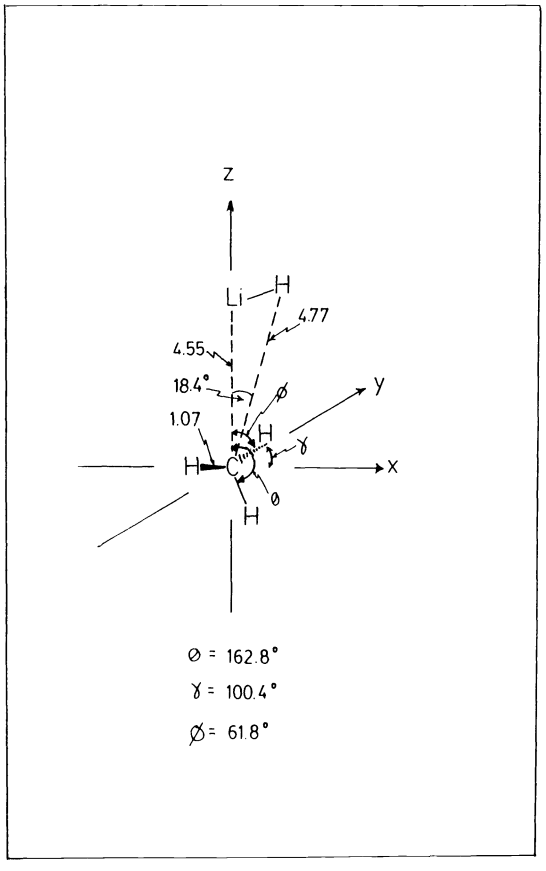


Figure 16 - Geometry optimized transition state (first order saddle point) for the side-on $C_s$ attack of a $^2P$ Li atom on $CH_4$ (Ref. 24).

adjacent C-H bond (Figure 16), with a methyl geometry rather similar to the $^2A_1$ ground state of $CH_3$....LiH. The geometry of the methyl part was found to be about 8° from a planar conformation in the transition state as compared with 7° for the $^2A_1$ ground state of $CH_3$....LiH.

The general conclusion that emerges from the calculations of the $^2P$ Li atom insertion reaction is that the activation barrier to insertion (Figure 17) involves the elongation of a C-H bond of $CH_4$ to form a species in which the hydrogen atom is essentially abstracted giving a methyl radical and lithium hydride. The insertion product $CH_3$...LiH results from the additional stabilization gained from the "single electron bond" between the methyl and lithium hydride moieties (Ref. 24).

Clearly much more work along these lines is necessary, with an extension to transition metal atoms and clusters in ground and electronically excited states, before one can begin to comprehend the chemisorption and C-H bond activation of saturated hydrocarbons on transition metal surfaces.

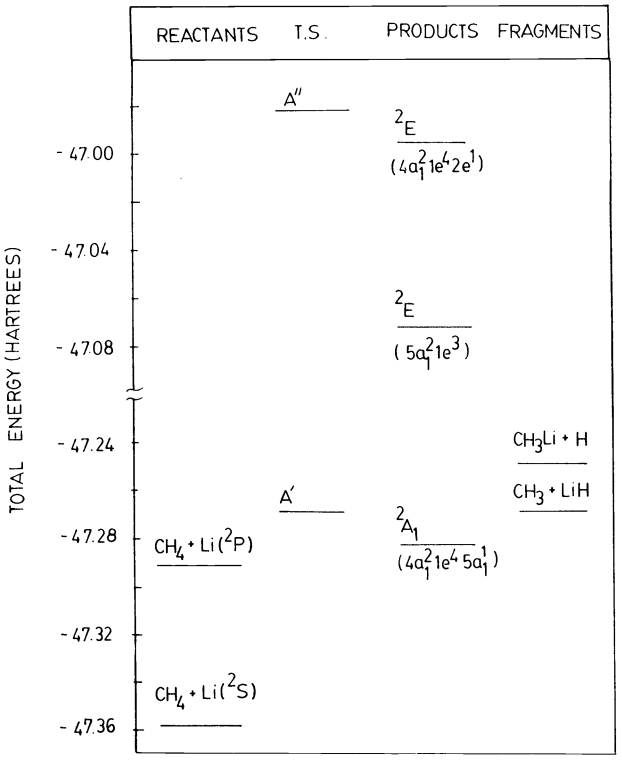


Figure 17 - The 3 - 21G basis set total energies (hartrees) for reactants (Li, $CH_4$), transition state ($CH_3LiH$, $C_s$), products ($CH_3...LiH$, $C_{3v}$) and fragments ($CH_3$,LiH; $CH_3$Li,H), Ref. 24).

ACKNOWLEDGEMENTS

The generous financial assistance of the Natural Sciences and Engineering Research Council of Canada's Strategic Energy Programme is greatly appreciated. We would like to thank Mr. H. Huber for valuable technical assistance at various stages of this research.

REFERENCES

1. E.L. Muetterties, Chem. Soc. Rev. (London), 11,283,(1982),(and references cited therein)
2. A.H. Janowicz and R.C. Bergman, J. Amer. Chem. Soc., 108, 3929, (1983) (and references cited therein).
3. R.C. Baetzold, J. Amer. Chem. Soc., 105, 4271,(1983) (and references cited therein).
4. G. A. Ozin, E.P. Kündig, D.F. McIntosh and M. Moskovits, J. Amer. Chem. Soc., 95, 7234, (1973).
5. G.A. Ozin, H. Huber, E.P. Kündig and M. Moskovits, J. Amer. Chem. Soc., 95, 332, (1973).
6. G.A. Ozin and A.J.L. Hanlan, Inorg. Chem.,16, 2848, (1977); 16, 2857, (1977).
7. G.A. Ozin, H. Huber and D.F. McIntosh, Inorg. Chem., 16, 3070, (1977).
8. G.A. Ozin, D.F. McIntosh, W.J. Power and R.P. Messmer, Inorg. Chem., 20, 1782, (1981).
9. G.A. Ozin, W. Klotzbücher, H. Kolari and J.G. Norman, Jr., Inorg. Chem., 16, 2871, (1977).
10. K.J. Klabunde and Y. Tanaka, J. Amer. Chem. Soc.,105, 3544, (1983).
11. H. Huber and G.A. Ozin, Inorg. Chem., 17, 155, 1978; G.A. Ozin, Faraday Symp. Chem. Soc. 14, 7, 1980; Angew. Chem. Int. Ed., Oct. (1983); G.A. Ozin and S.A. Mitchell, A.C.S. Symp. Ser., 211, 303, (1983) (and references cited therein).
12. D.H.W. Carstens, W. Brashear, D.R. Eslinger and D.M. Gruen, Appl. Spectros., 26, 184, (1972).
13. K.J. Zeringne, J.S. Emampour, J.C. Rivoal and M. Vala, J. Chem. Phys., 78, 2231, (1983) (and references cited therein).
14. G.A. Ozin and J.G. McCaffrey, J. Phys. Chem., (submitted).
15. (a) J. Kitaura, S. Obara and K. Morokuma, J. Amer. Chem. Soc., 103, 2891, (1981); A Sevin, Nouveau J. Chim., 5, 233, (1981); J.O. Noell and P.J. Hay, J.Amer. Chem. Soc., 104, 4578, (1982); (b) P.B. Chock and J. Halpern, J. Amer. Chem. Soc., 88, 3511, (1966); (c) G.J. Kubas, Los Alamos Report, (1983).

16. G.A. Ozin, and J.G. McCaffrey, J. Amer. Chem. Soc., (submitted).
17. G.L. Geoffroy and R.J. Pierantozzi, J. Amer. Chem. Soc., 98, 8054, (1976); G.L. Geoffroy and M.G. Bradley, Inorg. Chem., 17, 2410, (1978).
18. G.A. Ozin, D.F. McIntosh and J.G. McCaffrey, (in preparation).
19. G.A. Ozin and J.G. McCaffrey, (unpublished observations).
20. G.A. Ozin and J.G. McCaffrey, J. Amer. Chem. Soc., 104, 7351, (1982).
21. G.A. Ozin, J.G. McCaffrey and H. Huber, (unpublished observations); W.E. Billups, J.L. Margrave and R.H. Hauge, J. Amer. Chem. Soc., 102, 7393, (1980).
22. G.A. Ozin, D.F. McIntosh, S.A. Mitchell and G. Garcia-Prieto, J. Amer. Chem. Soc., 103, 1574, (1981); Pure and Appl. Chem., (1983) (in press); Angew. Chem. Int. Ed., (submitted).
23. J. Demuth, H. Ibach and S. Lehwald, Phys. Rev. Letters., 40, (1982); A.J. Schulz, J.M. Williams, R.R. Schrock, G.A. Rupprecht and J.D. Allman, J. Amer. Chem. Soc., 101, 1953, (1979) (and references cited therein).
24. J.G. McCaffrey, R.A. Poirier, G.A. Ozin and I.G. Csizmadia, J. Phys. Chem., (submitted)
25. L.Y. Tan and G.C. Pimentel, J. Chem. Phys., 48, 5202, (1968).
26. G.A. Ozin, A.J.L. Hanlan and W.J. Power, Inorg. Chem., 17, 3648, (1978).
27. S.P. Walch and C.W. Bauschlicher, Jr., J. Chem. Phys., 78, 4597, (1983) (and references cited therein).
28. B. Breithaupt, J.E. Hulse, D.M. Kolb, H.H. Rotermund, W. Schroeder and W. Schrittenlacher, Chem. Phys. Lett., 95, 513 (1983).